Channel Estimation and Environment Sensing of Slightly Distributed Scatterers Using A Spherical-wave Generalized Array Manifold Model

Yixiao Tong*, Guangzheng Jing*, Jingxiang Hong*, Ruiqi Zhou*, José Rodríguez-Piñeiro* and Xuefeng Yin*
*College of Electronics and Information Engineering, Tongji University, Shanghai, China,
{tyx2030828, Jing_Guangzheng, hongjx, 2033096, j.rpineiro, yinxuefeng}@tongji.edu.cn

***Abstract*—This paper proposes a Spherical-wave Generalized Array Manifold Space-Alternating Generalized Expectation-maximization (SW-GAM-SAGE) algorithm to jointly estimate conventional channel parameters and physical characteristics of slightly distributed scatterers (SDSs). By integrating the Spherical-wave GAM (SW-GAM) model into the spherical-wave SAGE (SW-SAGE) framework, the algorithm enhances parameter estimation accuracy under strict SDS constraints. Monte Carlo simulations confirm its superior performance in high Signal-to-Noise Ratio (SNR) environments. Experimental validation using indoor measurement data reveals that both SW-SAGE and SW-GAM-SAGE achieve equivalent precision in extracting multipath components (MPCs) and SDSs, respectively. To address near-field sensing limitations, a hybrid channel model combining spherical-wave MPCs with SDSs is further proposed, whose efficacy is rigorously verified through practical measurements. This work advances near-field integrated sensing and communication (ISAC) channel modeling and provides a foundational framework for sixth generation (6G) system design, bridging theoretical innovation with practical sensing-communication integration.**

***Index Terms*—Channel parameter estimation, ISAC, spherical wave front, near-field**

I. Introduction

Integrated sensing and communication (ISAC) has emerged as a critical enabler for the sixth generation (6G) wireless systems, necessitating enhanced capabilities in environmental sensing of both signal sources and scatterers. This paradigm shift elevates the importance of physics-based channel modeling that accurately incorporates geometric characteristics of scattering objects, including their spatial distributions and dimensional attributes, derived from advanced sensing techniques [1].

Contemporary localization methodologies employing spherical-wavefront-based parametric models demonstrate promising results in estimating first/last-hop scatterer positions through high-resolution parameter estimation (HRPE) with multi-antenna synchronized systems. These approaches explicitly account for the wavefront curvature by modeling the distance-dependent relationship between scatterers and antenna arrays. Recent advancements in spherical-wave-based localization have extended operational capabilities through various strategies: leveraging geometric constraints as prior information [2], modeling dense multi-path componentss (DMCs) [3], [4], exploiting time-difference-of-arrival measurements from distributed/mobile receivers [5]–[7], and implementing triangulation principles [8]. Nevertheless, current channel estimation frameworks exhibit fundamental limitations in characterizing the spatial extent of scattering objects, particularly in quantifying the physical dimensions of scatterers or resolving the dispersion characteristics of slightly distributed scatterer (SDS) [9]–[11].

To address these limitations, a prior parametric channel model is integrated into generalized array manifold (GAM) [9] manifolds architecture, and a called Spherical-wave Generalized Array Manifold Space-Alternating Generalized Expectation-maximization (SW-GAM-SAGE) algorithm is proposed. The proposed model and the corresponding algorithm exhibits the ability of estimating the channel parameters and obtaining the spreading of SDSs. Compared to other conventional algorithms, the proposed algorithm is based on spherical-wave-based model and considers a Taylor series expansion of static DMCs not only in azimuth and elevation domains, but also in distance domain between the reference antennas of the Tx/Rx array and the first/last-hop scatterers(hereinafter referred to as first/last-hop distance).

The remainder of this work is organized as follows: Section II derives the Spherical-wave GAM (SW-GAM) channel model. The SW-GAM-SAGE algorithm is also derived using the space-alternating generalized expectation-maximization (SAGE) structure. Section III describes the simulation result for prove the viability of the algorithm. Section IV provides reasonable results in measurement-based. Section V proposed a mixed channel model. Finally, Section VIconcludes the paper.

II. GAM Signal Model and SW-GAM-SAGE Algorithm

A. GAM Signal Model for MIMO Systems

Let consider a single-input multiple-output (SIMO) system in which the Rx is equipped with a uniform planar array (UPA) with M antenna elements. The frequency response

This work was supported by the Ministry Of Science and Technology (MOST) of China under the grant 2022YF-B2503403; the Special Funds for the Basic Research of Tongji University under the grant 22120220669 and the Special Funds of the Tongji University for "Sino-German Cooperation 2.0 Strategy" under the grant ZD2023012. The authors would like to thank the colleagues at the Sino-German Center of Intelligent Systems, and the Shanghai Institute of Intelligent Science and Technology, Tongji University.

$y_{\text{SDS},m}(f)$ received by the mth Rx antenna ($m = 1, ..., M$) in a single-SDS propagation scenario can be viewed as the total contribution of multiple spherical-wave paths:

$$y_{\text{SDS},m}(f) = \sum_{\ell=1}^{L} \alpha_\ell c_{\text{Rx},m}(\mathbf{\Omega}'_{\text{Rx},\ell}) \exp\{-j2\pi f \tau_\ell\} \exp\{-j2\pi f[\frac{\|d_{\text{Rx},\ell}\mathbf{\Omega}_{\text{Rx},\ell} - \mathbf{r}_{\text{Rx},m}\| - d_{\text{Rx},\ell}}{c_0}]\} + \omega_m(f), \quad (1)$$

where L represents total number of propagation paths, $\mathbf{\Omega}_{\text{Rx},\ell} = [\sin(\theta)\cos(\phi), \sin(\theta)\sin(\phi), \cos(\theta)]$, α_ℓ and τ_ℓ represent the direction of arrival (DoA) at the reference antenna, complex amplitude, and propagation delay of ℓth path, respectively; θ and ϕ denote the Elevation of Arrival (EoA) and Azimuth of Arrival (AoA). $d_{\text{Rx},\ell}$ is the last-hop distance for the ℓth path. $\mathbf{\Omega}'_{\text{Rx},\ell} = (\bar{d}\bar{\mathbf{\Omega}} - \mathbf{r}_m)/\|\bar{d}\bar{\mathbf{\Omega}} - \mathbf{r}_m\|$ is the DoA at the mth antenna. $c_{\text{Rx},m}$ denotes the mth Rx antenna response. $\mathbf{r}_{\text{Rx},m}$ represents the position vector of the mth antenna on the Rx array, and $\omega_m(f)$ is white Gaussian noise with variance σ_ω^2.

Similarly to the definition of SDS under the plane-wave front assumption [11], an SDS under spherical-wave front assumption can be expressed by $\theta_\ell = \bar{\theta}_\ell + \tilde{\theta}_\ell$, $\phi_\ell = \bar{\phi}_\ell + \tilde{\phi}_\ell$, $d_\ell = \bar{d}_\ell + \tilde{d}_\ell$. $\bar{(\cdot)}$ and $\tilde{(\cdot)}$ denote nominal value and deviations, respectively. The deviations of the three parameters are independent to each other. Then, the first-order Taylor series expansion at a given parameter of ℓth path can be obtained, and Eq. (1) yields the GAM model [12] as:

$$y_{\text{SDS},m}(f) = [A\ B\ C\ D] \cdot [F\ F'_\theta\ F'_\phi\ F'_d]^{\text{T}} + \omega_m(f), \quad (2)$$

with

$$A = \sum_{\ell=1}^{L} \alpha_\ell, B = \sum_{\ell=1}^{L} \alpha_\ell \tilde{\theta}_\ell, C = \sum_{\ell=1}^{L} \alpha_\ell \tilde{\phi}_\ell, D = \sum_{\ell=1}^{L} \alpha_\ell \tilde{d}_\ell, \quad (3)$$

and

$$F(f;\bar{\theta},\bar{\phi},\bar{d},\tau) = \exp\{-j2\pi f\tau\} G_{\text{Rx},m}(f;\bar{\theta},\bar{\phi},\bar{d}), \quad (4)$$

$$F_d(f;\bar{\theta},\bar{\phi},\bar{d},\tau) = \exp\{-j2\pi f\tau\} G_{\text{Rx},m}(f;\bar{\theta},\bar{\phi},\bar{d}) \left[\frac{c_m(\bar{\mathbf{\Omega}}')j2\pi f}{c_0}\left(1 - \frac{\bar{d} - \bar{\mathbf{\Omega}}^{\text{T}}\mathbf{r}_m}{\|\bar{d}\bar{\mathbf{\Omega}} - \mathbf{r}_m\|}\right) + \frac{\partial c_m(\mathbf{\Omega}')}{\partial d}\Big|_{d=\bar{d},\theta=\bar{\theta},\phi=\bar{\phi}}\right],$$

$$F_\theta(f;\bar{\theta},\bar{\phi},\bar{d},\tau) = \exp\{-j2\pi f\tau\} G_{\text{Rx},m}(f;\bar{\theta},\bar{\phi},\bar{d}) \left[\frac{c_m(\bar{\mathbf{\Omega}}')j2\pi f\bar{d}\mathbf{r}_m^{\text{T}}\frac{\partial\mathbf{\Omega}}{\partial\theta}\Big|_{\theta=\bar{\theta},\phi=\bar{\phi}}}{c_0\|\bar{d}\bar{\mathbf{\Omega}} - \mathbf{r}_m\|} + \frac{\partial c_m(\mathbf{\Omega}')}{\partial\theta}\Big|_{d=\bar{d},\theta=\bar{\theta},\phi=\bar{\phi}}\right],$$

$$F_\phi(f;\bar{\theta},\bar{\phi},\bar{d},\tau) = \exp\{-j2\pi f\tau\} G_{\text{Rx},m}(f;\bar{\theta},\bar{\phi},\bar{d}) \frac{1}{\sin(\bar{\theta})} \left[\frac{c_m(\bar{\mathbf{\Omega}}')j2\pi f\bar{d}\mathbf{r}_m^{\text{T}}\frac{\partial\mathbf{\Omega}}{\partial\phi}\Big|_{\theta=\bar{\theta},\phi=\bar{\phi}}}{c_0\|\bar{d}\bar{\mathbf{\Omega}} - \mathbf{r}_m\|} + \frac{\partial c_m(\mathbf{\Omega}')}{\partial\phi}\Big|_{d=\bar{d},\theta=\bar{\theta},\phi=\bar{\phi}}\right],$$

where

$$G_{\text{Rx},m}(f;\bar{\theta},\bar{\phi},\bar{d}) = \exp\left\{-j2\pi f\frac{\|d_\ell\mathbf{\Omega}_\ell - \mathbf{r}_m\| - d_\ell}{c_0}\right\}. \quad (5)$$

In a scenario with a total of K SDSs, Eq. (2) can be re-written in matrix form as:

$$\mathbf{Y}(f) = \sum_{k=1}^{K} \mathbf{F}_k\boldsymbol{\xi}_k + \mathbf{W}(f), \quad (6)$$

where $\mathbf{Y}(f) \in \mathbb{C}^{MS\times 1}$, $\mathbf{F}_k \in \mathbb{C}^{MS\times 4}$, $\boldsymbol{\xi}_k \in \mathbb{C}^{4\times 1}$, with

$$\mathbf{F}_k = [F_k, F_{\theta,k}, F_{\phi,k}, F_{d,k}], \boldsymbol{\xi}_k = [A_k, B_k, C_k, D_k]^{\text{T}}. \quad (7)$$

The values of $\mathbf{F}_k$ and $\boldsymbol{\xi}_k$ are given by using $\theta_k, \phi_k, d_k, \tau_k$ to replace the values of θ, ϕ, d, τ in Eq. (3) and Eq. (4). Then the unknown parameters set $\boldsymbol{\theta}_k \in \mathbf{\Theta} = [\boldsymbol{\theta}_1, \boldsymbol{\theta}_2, ..., \boldsymbol{\theta}_K]^{\text{T}}$ in Eq. (6) is given as:

$$\boldsymbol{\theta}_k = [\tau_k, \bar{\theta}_k, \bar{\phi}_k, \bar{d}_k, A_k, B_k, C_k, D_k]. \quad (8)$$

By estimating the parameters for L paths in K SDSs, the obtainment of both conventional channel parameters and spreading of SDSs can be achieved.

B. Proposed SAGE-based Channel Estimation

In the SW-GAM-SAGE framework, the admissible hidden-data space can be expressed as:

$$\mathbf{Y}_k(f) = \mathbf{F}_k\boldsymbol{\xi}_k + \mathbf{W}(f). \quad (9)$$

In the expectation (E-) step [13] of the SAGE algorithm, the objective function Q at the ith iteration, and given the realization $\mathbf{y}(f)$, is written as:

$$\begin{aligned} Q(\boldsymbol{\theta}_k|\hat{\mathbf{\Theta}}^{i-1}) &= E[\Lambda(\mathbf{\Theta};\mathbf{Y}_k)|\mathbf{Y}(f) = \mathbf{y}(f), \hat{\mathbf{\Theta}}^{i-1}] \quad (10)\\ &= -MS\ln\sigma_w^2 - \frac{1}{\sigma_w^2}\left\|\hat{\mathbf{y}}^{i-1}(f) - \mathbf{F}_k\boldsymbol{\xi}_k\right\|^2 \\ &\propto -\left\|\hat{\mathbf{y}}^{i-1}(f) - \mathbf{F}_k\boldsymbol{\xi}_k\right\|^2, \end{aligned}$$

where

$$\hat{\mathbf{y}}_k^{i-1}(f) = \mathbf{y}(f) - \sum_{k'=1,k'\neq k}^{K} \widehat{\mathbf{F}}_{k'}^{i-1}\hat{\boldsymbol{\xi}}_{k'}^{i-1} \quad (11)$$

is an estimation of $\mathbf{Y}_k(f)$ when $\mathbf{y}(f)$ is obtained and $\boldsymbol{\theta} = \hat{\boldsymbol{\theta}}^{i-1}$. In the maximization (M-) step [13], the unknown parameter set for the ith iteration can be given by:

$$\hat{\boldsymbol{\theta}}_k^i = \arg\max\{Q(\boldsymbol{\theta}_k|\hat{\boldsymbol{\theta}}^{i-1})\}. \quad (12)$$

By setting $\partial\Lambda(\mathbf{\Theta};\mathbf{X}_k)/\partial\hat{\boldsymbol{\xi}}$ to 0(similarly to the procedure in [14]), the estimation of $\hat{\boldsymbol{\xi}}_k^i$ can be derived as:

$$\hat{\boldsymbol{\xi}}_k^i = (\widehat{\boldsymbol{F}}_k^{i\,\text{H}}\widehat{\boldsymbol{F}}_k^i)^{-1}\widehat{\boldsymbol{F}}_k^{i\,\text{H}}\hat{\mathbf{y}}_k^{i-1}(f). \quad (13)$$

In the implementation of the SAGE algorithm, the multi-dimensional maximization in Eq. (12) is replaced by a so-called coordinate-wise updating procedure similar to that used in [8], [15]

$$\begin{aligned} \hat{\tau}_k^i &= \arg\max_{\tau_k}\{z(\tau_k, \hat{\bar{\theta}}_k^{i-1}, \hat{\bar{\phi}}_k^{i-1}, \hat{\bar{d}}_k^{i-1}; \hat{\mathbf{y}}_k^{i-1}(f))\}, \quad (14)\\ \hat{\theta}_k^i &= \arg\max_{\bar{\theta}_k}\{z(\hat{\tau}_k^i, \bar{\theta}_k, \hat{\bar{\phi}}_k^{i-1}, \hat{\bar{d}}_k^{i-1}; \hat{\mathbf{y}}_k^{i-1}(f))\},\\ \hat{\phi}_k^i &= \arg\max_{\bar{\phi}_k}\{z(\hat{\tau}_k^i, \hat{\bar{\theta}}_k^i, \bar{\phi}_k^{i-1}, \hat{\bar{d}}_k^{i-1}; \hat{\mathbf{y}}_k^{i-1}(f))\},\\ \hat{d}_k^i &= \arg\max_{\bar{d}_k}\{z(\hat{\tau}_k^i, \hat{\bar{\theta}}_k^i, \hat{\bar{\phi}}_k^i, \bar{d}_k; \hat{\mathbf{y}}_k^{i-1}(f))\}, \end{aligned}$$

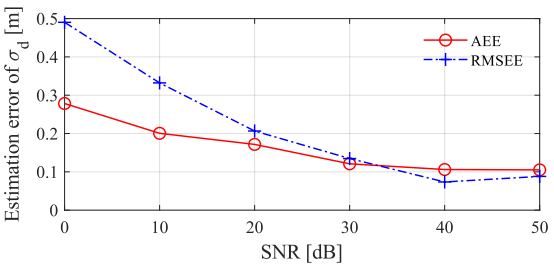

Fig. 1. AEE and RMSEE of σ_{d} vs. Signal-to-Noise Ratio (SNR).

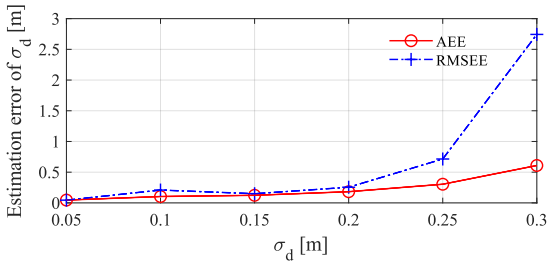

Fig. 2. AEE and RMSEE of σ_{d} vs. distance expansion.

where

$$z(\mathbf{F}_k;\hat{\mathbf{y}}_k(f)) = \hat{\mathbf{y}}_k(f)^{\mathrm{H}}\mathbf{F}_k(\mathbf{F}_k{}^{\mathrm{H}}\mathbf{F}_k)^{-1}\mathbf{F}_k{}^{\mathrm{H}}\hat{\mathbf{y}}_k(f). \quad (15)$$

After estimating $\hat{\boldsymbol{\xi}}_k$, the AoA spread $\sigma_{\tilde{\phi}}$, EoA $\sigma_{\tilde{\theta}}$, and the last-hop distance spread $\sigma_{\tilde{d}}$ of the k-th SDS can be calculated as [10], [12]:

$$\sigma_{\tilde{\phi}} = |C_k|^2/|A_k|^2, \sigma_{\tilde{\theta}} = |B_k|^2/|A_k|^2, \sigma_{\tilde{d}} = |D_k|^2/|A_k|^2. \quad (16)$$

III. SIMULATION RESULTS

For proving the viability of the proposed algorithm, Monte-Carlo simulations in a single-SDS scenario are performed. In simulation, the environment is time-invariant and the Rx is equipped with a uniform 8×8 planar array consisting of 64 omnidirectional antennas with 0.5λ interval. The SDS consists of $L = 1000$ sub-scatterers. The position of the SDS is set to be 2 m away from the reference antenna, while the EoA and AoA are set to 45°. The random elements characterizing the contribution of sub-scatterers to the channel response are generated in the following way: the complex gain of each sub-scatterer has the same amplitude and different random phase. Their AoAs, EoAs, and distances are i.i.d. The carrier frequency is 3.5 GHz and the bandwidth is 100 MHz.

The parameters are considered in order to evaluate the performance of the method: *1)*different SNR and *2)*different distance spread $\sigma_{\tilde{d}}$ of the SDSs. Firstly, the effect of different SNR on the estimation of the distance spread $\sigma_{\tilde{d}}$ in the single-SDS is considered for the SNR range between 0 dB and 40 dB. It can be seen from Fig. 1 that the average estimation error (AEE) and root-mean-square-estimation-error (RMSEE) of the $\sigma_{\tilde{d}}$ estimated are decreasing and converging to 0 with the SNR increasing. As expected, the estimation of $\sigma_{\tilde{d}}$ is more reliable in a scenario with higher SNR. Secondly, we consider the effect of σ_d for the single-SDS. The $\sigma_{\tilde{d}}$ is set from 0.05 m to 0.3 m. Fig. 2 shows that the AEE and RMSEE of the estimated of $\sigma_{\tilde{d}}$ grow with $\sigma_{\tilde{d}}$ increasing. This indicates that the performance of the estimator decreases with the size of the SDS, since the assumptions of SDS that SDS is the sum of multiple sub-scatterers with slightly different parameter become invalid [12].

TABLE I
MEETING ROOM SIMO MEASUREMENT CONFIGURATION.

Parameter	Value
Frequency	$12-14$ GHz
Bandwidth	2 GHz
Frequency point	251
Transmitted Power	0 dBm
Antennas Type	Bi-conical
Antenna Gain	8 dBi
Size of Antenna Array	32×32 planar array

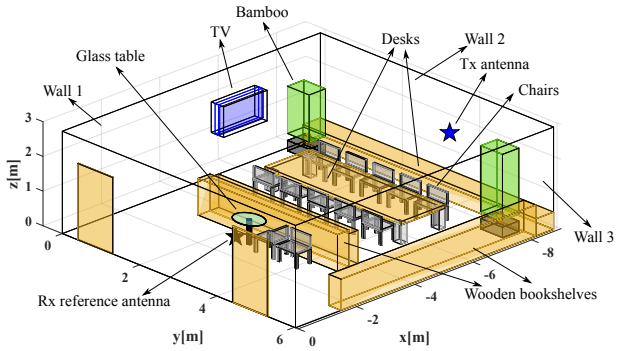

Fig. 3. Schematic diagram of measurement scenario.

IV. ANALYSIS OF MEASUREMENT DATA

The measurement was conducted in a meeting room with a size of $8.84 \times 6.03 \times 2.95\,\mathrm{m}^3$ at Tongji University, Shanghai, China. Two wide-band antennas were used to build a SIMO system. The Rx was equipped with a 32×32 planar array perpendicular to the floor. Inter-element distance was set to half wavelength of the maximum frequency. 251 frequency points ranging from 12 GHz to 14 GHz were measured. The parameters of the measurement configuration are shown in TABLE I and Fig. 3 shows the schematic diagram of the measurement scenario.

In order to eliminate the frequency selectivity of wide band, the measurement data was split into two parts to be estimated at $12-13$ GHz and $13-14$ GHz. Then, the results are superimposed. Both the spherical-wave SAGE (SW-SAGE) and the SW-GAM-SAGE algorithms are used for estimating the parameters of the multipath components (MPCs) or SDSs, respectively. First, the two algorithms are both set up to estimated 30 paths. Additionally, considering the larger number of parameters used in the SW-GAM model w.r.t the spherical-wave model, another estimation using the SW-SAGE

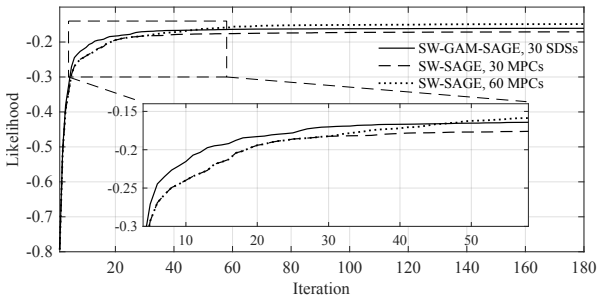

Fig. 4. Likelihood of SW-SAGE algorithm and SW-GAM-SAGE algorithm.

algorithm is set up to estimated 60 paths, in order to make the number of parameters consistent.

Fig. 4 shows the likelihood curve. The curve of the SW-GAM-SAGE algorithm begins to converge after about 40 iterations, while the SW-SAGE algorithm needs 50 and 80 iterations to converge for different settings. Since the SW-GAM-SAGE algorithm extracts 30 SDSs, the likelihood value is higher than that of the SW-SAGE with 30 paths. Meanwhile, the SW-SAGE algorithm needs to estimate about $45-50$ paths to achieve a similar convergence value of the likelihood function. It can be concluded that the SW-GAM-SAGE algorithm can extract more channel components with fewer paths.

Fig. 5 shows the estimation results of the SW-GAM-SAGE and SW-SAGE algorithms, as well as the last hop scatterers mapped in 3D scenario. In particular, the scatterers plot for the SW-GAM-SAGE algorithm constitute the central point of each SDS. It can be seen from Fig. 5 that most of the power is distributed in three areas marked by boxes labeled as: *Area 1*: line-of-sight (LoS) component; *Area 2*: MPCs caused by Wall 2; *Area 3*: MPCs caused by the corner and bamboo. The distribution of scatterers in Area 3 is more diffuse. This may be due to the more complex and irregular physical shapes at this area. At the same time, as we can see from Fig. 5, there are some scatterers outside the room(including Area 4). The reasons are specifically discussed in [1] and can be summarized as follows: *1)* the spherical-wave model is not always accurate; *2)* the Rx antenna does not provide enough angular resolution; *3)* there are many specular reflections in the environment.

V. HYBRID CHANNEL MODEL

Fig. 6 shows the Cumulative Distribution Function (CDF) of the estimated distance spread. Some large distance spread values caused by the mismatch between propagation mechanisms and the SW-GAM model can be appreciated. These mismatching issue might be caused by low SNR of some MPCs, complex environment and others. In order to address this mismatching issue, we can set a threshold to separate SDSs. SDSs whose σ_d is larger than the threshold cannot be considered as SDSs, but as spherical-wave MPCs. Therefore

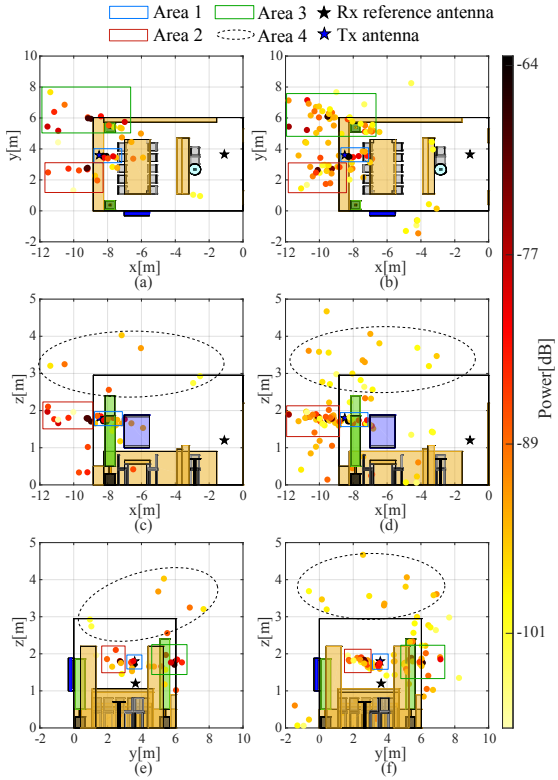

Fig. 5. Estimation results of SW-GAM-SAGE and SW-SAGE. *Left side (a, c, e): results of SW-GAM-SAGE at XY , XZ and YZ view. Right side (b, d, f): results of SW-SAGE at XY , XZ and YZ view.*

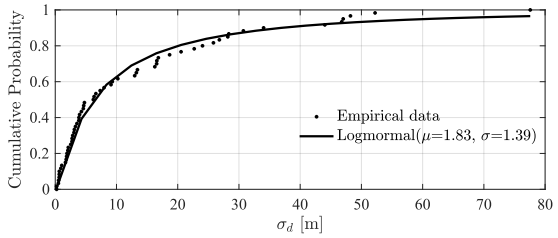

Fig. 6. CDF of distance expansion (σ_d).

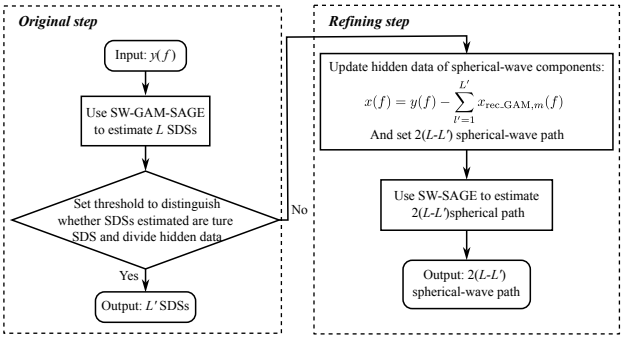

Fig. 7. Flow chart of the algorithm for hybrid channel.

the hybrid channel model can be extended as:

$$y(f)=\sum_{l'=1}^{L'} x_{\text{rec\_GAM},l'}(f)+\sum_{n=1}^{N} x_{\text{rec\_SW},m}(f)+w(f). \quad (17)$$

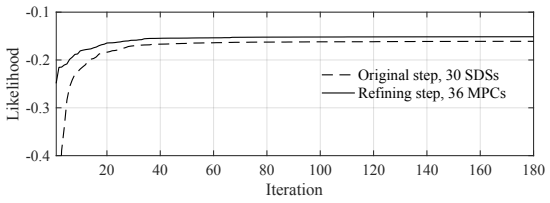

Fig. 8. Likelihood of original step and refining step.

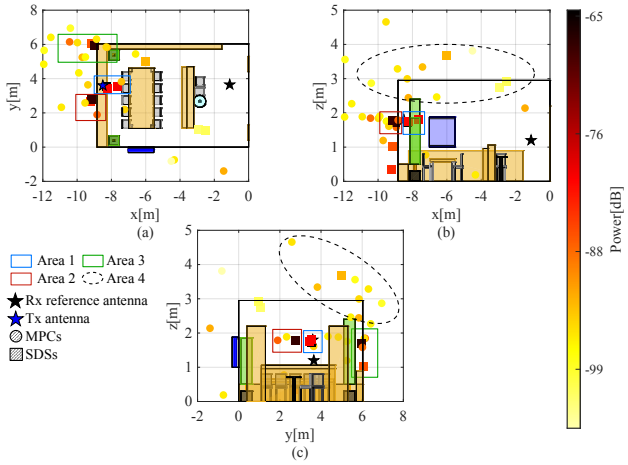

Fig. 9. Estimation results of SW-GAM-SAGE based on mix channel model.

$x_{\text{rec\_GAM},l'}(f)$ is the component reconstructed by the SW-GAM model, and $x_{\text{rec\_SW},m}(f)$ is the component reconstructed by the spherical-wave model. Fig. 7 gives the flow chart of the algorithm for the hybrid channel model. The algorithm is divided into two parts. Firstly, the SW-GAM-SAGE algorithm is used. After the convergence of the likelihood function, $\sum_{l'=1}^{L'} x_{\text{rec\_GAM},l'}(f)$ is reconstructed by using the estimated SDSs with σ_d smaller than a given threshold. Then, the hidden data can be updated by:

$$x(f) = y(f) - \sum_{l'=1}^{L'} x_{\text{rec\_GAM},l'}(f). \tag{18}$$

Since the SW-GAM model for a SIMO system has 12 parameters and spherical-wave model 6, the number of spherical-wave MPCs needed to be estimated is larger than $L - L'$. To keep the number of parameters consistent, the number of spherical-wave MPCs is set to $2(L - L')$ in this paper. Fig. 8 shows the likelihood of the original step and the refining step when using measurement data. It can be seen that the refining step improves the convergence value of the likelihood function. Fig. 9 shows the estimation results. The distribution of scatterers is similar to the results mentioned above and the power distribution is more concentrated in four areas. This shows that the model is more consistent with the real channel and more channel components can be extracted for the same number of parameters.

VI. CONCLUSIONS

This paper proposes a SW-GAM-SAGE algorithm for joint estimation of the conventional channel parameters and the SDSs physical information. By incorporating the GAM model into the SW-SAGE framework, the proposed method demonstrates high performance in high SNR scenarios under a strict SDS assumption, as validated by Monte Carlo simulations. Both SW-SAGE and SW-GAM-SAGE achieve comparable accuracy in extracting MPCs and SDSs from indoor measurement data, respectively, confirming the feasibility of the approach. To further improve sensing accuracy, we introduce a hybrid channel model integrating spherical-wave MPCs and SDSs, proving its accuracy with measurement data. This work advances on the near-field ISAC channel estimation and lays a foundation for future 6G sensing systems.

REFERENCES

[1] G. Jing, J. Hong, X. Yin, J. Rodríguez-Piñeiro, and Z. Yu, "Measurement-based 3-d channel modeling with cluster-of-scatterers estimated under spherical-wave assumption," *IEEE Transactions on Wireless Communications*, vol. 22, pp. 5828–5843, 2023.

[2] J. Hong, J. Rodríguez-Piñeiro, X. Yin, and Z. Yu, "Joint channel parameter estimation and scatterers localization," *IEEE Transactions on Wireless Communications*, vol. 22, pp. 3324–3340, 2023.

[3] J. Salmi, A. Richter, and V. Koivunen, "Detection and tracking of mimo propagation path parameters using state-space approach," *IEEE Transactions on Signal Processing*, vol. 57, pp. 1538–1550, 2009.

[4] T. Jost, W. Wang, U.-C. Fiebig, and F. Perez-Fontan, "Detection and tracking of mobile propagation channel paths," *IEEE Transactions on Antennas and Propagation*, vol. 60, pp. 4875–4883, 2012.

[5] R. Mendrzik, F. Meyer, G. Bauch, and M. Z. Win, "Enabling situational awareness in millimeter wave massive mimo systems," *IEEE Journal of Selected Topics in Signal Processing*, vol. 13, pp. 1196–1211, 2019.

[6] E. Leitinger, F. Meyer, F. Hlawatsch, K. Witrisal, F. Tufvesson, and M. Z. Win, "A belief propagation algorithm for multipath-based slam," *IEEE Transactions on Wireless Communications*, vol. 18, pp. 5613–5629, 2019.

[7] E. Leitinger, S. Grebien, and K. Witrisal, "Multipath-based slam exploiting aoa and amplitude information." Shanghai, China: IEEE, 2019, pp. 1–7.

[8] X. Yin, S. Wang, N. Zhang, and B. Ai, "Scatterer localization using large-scale antenna arrays based on a spherical wave-front parametric model," *IEEE Transactions on Wireless Communications*, vol. 16, pp. 6543–6556, 2017.

[9] N. Zhang, X. Yin, L. Tian, W. Duan, and S. R. Boqué, "Performance evaluation of interference cancellation using a generalized-array-manifold model." Washington, DC, USA: IEEE, 2014, pp. 670–675.

[10] P. Zhu, J. Rodriguez-Pineiro, X. Yin, G. Li, C. A. Gutierrez, and X. Li, "Slight-distributed-scatterer-based time-varying channel modeling for vehicular environments." Singapore, Singapore: IEEE, 2024, pp. 1–6.

[11] G. Jing, J. Hong, X. Yin, J. Rodríguez-Piñeiro, and Z. Yu, "Elaa channel characterization with parameter estimation based on a generalized array manifold model," *Electronics*, vol. 11, no. 21, 2022. [Online]. Available: https://www.mdpi.com/2079-9292/11/21/3442

[12] X. Yin and B. Fleury, "Nominal direction and direction spread estimation for slightly distributed scatterers using the sage algorithm," vol. 1. Stockholm, Sweden: IEEE, 2005, pp. 25–29 Vol. 1.

[13] J. Fessler and A. Hero, "Space-alternating generalized expectation-maximization algorithm," *IEEE Transactions on Signal Processing*, vol. 42, pp. 2664–2677, 1994.

[14] B. Fleury, M. Tschudin, R. Heddergott, D. Dahlhaus, and K. I. Pedersen, "Channel parameter estimation in mobile radio environments using the sage algorithm," *IEEE Journal on Selected Areas in Communications*, vol. 17, pp. 434–450, 1999.

[15] G. Jing, J. Hong, J. Rodríguez-Piñeiro, X. Yin, Z. Yu, J. He, and X. Li, "Spatial transformation imaging in terahertz band: A successive interference cancellation approach," *IEEE Wireless Communications Letters*, vol. 12, pp. 1414–1418, 2023.